(Received 13 November 2025, Accepted 18 December 2025, Scheduled 18 January 2026)

Transmission-Line Dual-Band Absorptive Bandstop Filter with Two Input Lossy Step-Impedance Stubs

Jiapei Dong[1,2], Xiaoying Zuo[1,2,*], Mengxin He[1,2], Yajian Li[1,2], Juntao Cao[1,2], and Zelin Sun[1,2]

[1]*Laboratory for Sensor, Beijing Information Science & Technology University, Beijing 100192, China*
[2]*School of Applied Science, Beijing Information Science & Technology University, Beijing 100192, China*

ABSTRACT: In this paper, a novel planar dual-band absorptive band-stop filter (ABSF) based on transmission lines is proposed. The filter structure is composed of multiple transmission lines and two chip resistors, which endows it with distinct advantages, including multiple transmission zeros, high-selectivity dual-band-stop performance. Through formula derivations, the specific positions of the four transmission zeros within the operating frequency are precisely determined. Experimental measurement results demonstrate that the -10 dB fractional bandwidth of the first stopband is 50.27% (from 0.7 GHz to 1.17 GHz), while that of the second stopband reaches 13.18% (from 3.33 GHz to 3.8 GHz). Across the entire frequency, the insertion loss S_{21} achieves a minimum of -45.20 dB at 1 GHz, and the return loss S_{11} attains a maximum of -10.27 dB at 3.94 GHz. The physical dimensions of the filter are 102 mm $\times$ 26 mm ($0.77\lambda_0 \times 0.20\lambda_0$).

1. INTRODUCTION

Planar band-stop filters with various performances play an important role in radio communications. In fact, to suppress interference signals and shield specific frequency bands, the main working area of band-stop filters is concentrated on the radio frequency front. When microstrip transmission lines are used, a reconfigurable band-stop filter capable of covering multiple frequency bands by switching the states of PIN diodes is reported in [1]. Obviously, in order to achieve a high quality factor characteristic of the band-stop filter, a new type of band-stop filter with a Surface Acoustic Wave (SAW) resonator cascaded with a transmission line is mentioned in [2]. There is no doubt that the size of a band-stop filter is a key performance indicator that requires focused attention. It is reported in [3] that the integration of two band-stop components, namely defected microstrip structure (DMS) and defected ground structure (DGS), in the vertical dimension can significantly reduce the size of traditional band-stop filters. To solve the challenge of radio frequency co-site interference, a tunable band-stop filter for airborne tactical communication is proposed in [4]. Through the methods described in [5, 6], the filtenna is endowed with narrow bandwidth and high selectivity by integrating filter functionality into the antenna structure.

With the development of modern radio communication, absorptive band-stop filters have become essential components for suppressing specific signal frequency bands, absorbing the unnecessary signal, and reducing interference to the system. Compared with traditional band-stop filters, absorptive band-stop filters convert the absorbed energy into thermal energy through internal resistive elements instead of reflecting it back to the signal source. This can greatly avoid the impact of standing waves and impedance mismatch caused by reflected signals, thereby enhancing the system's stability. It is evident that the absorption performance can be achieved by means of a load resistor. When coupled lines are adopted, a compact broadband absorptive band-stop filter based on coupled lines was reported in [7]. Nowadays, absorptive bandstop filters with broadband impedance matching have become a research focus. In [8], a method using distributed element resonators to design absorptive band-stop filters is discussed, and the proposed structure can achieve broadband impedance matching with a flat passband at both ports. However, when designing high-order absorptive band-stop filters using traditional distributed elements, it is inevitable to increase the number of loads. Band-stop filters that simultaneously exhibit absorptive performance and extended upper passband capability have become a relatively novel research direction nowadays. In [9], an extended upper passband absorptive band-stop filter capable of achieving excellent broadband impedance matching performance is reported. In [10], an ultra-compact broadband absorptive band-stop filter adopting a thin-film integrated passive device technology is introduced. This structure enhances frequency selectivity by generating additional transmission zeros through series inductors and capacitor resonators. In [11], the design of a novel tunable monolithic microwave integrated circuit (MMIC)-based quasi-absorptive band-stop filter with ultra-high stopband rejection is discussed. In this reference, an asynchronous tuning method is adopted to enhance the robustness of the design and achieve ultra-high stopband attenuation over a wide tuning range. A novel broadband absorptive band-stop filter with multiple transmission zeros is mentioned in [12], in which a coupled-line structure is adopted, which can be used to increase the number of transmission zeros of the absorptive band-stop filter and achieve excellent frequency selectivity. Moreover, for absorptive band-stop filters, achieving tunable

* Corresponding author: Xiaoying Zuo (zuoxiaoying03@163.com).

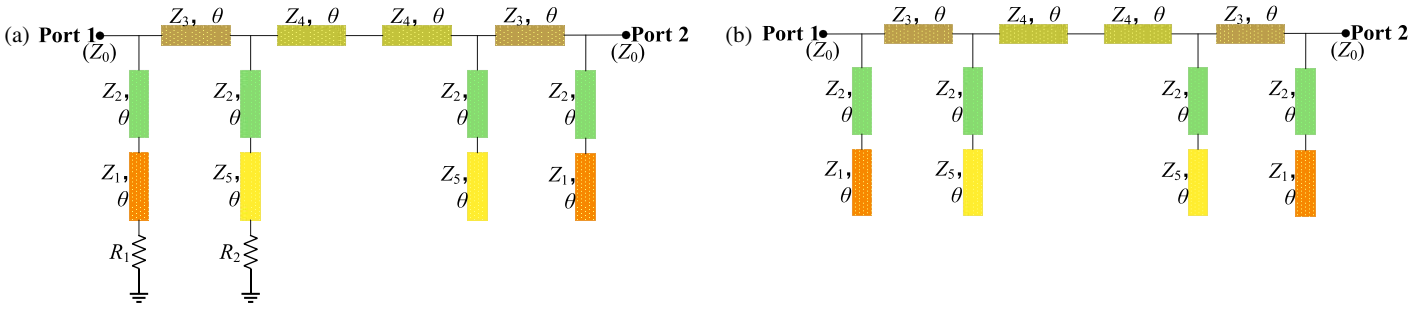

FIGURE 1. (a) Circuit topology of the proposed planar absorptive filter. (b) Circuit topology of the dual-band bandstop filter.

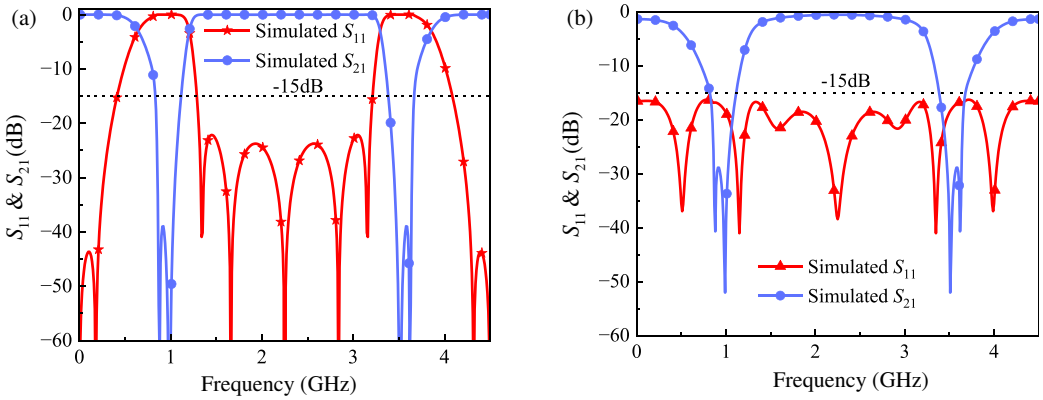

FIGURE 2. Ideal simulated S-parameters of bandstop filter. (a) Without R_1 & R_2. (b) With R_1 & R_2.

performance or switchable bandpass-bandstop performance is also a current research hotspot. A frequency-tunable absorptive band-stop filter is introduced in [13]. Methods for realizing bandpass-bandstop switching are described in [14, 15].

Modern radio communications often need to operate in multiple frequency bands simultaneously. However, the realization of multi-band operation has not been addressed in [7–15]. In [16], an innovative tunable wideband band-stop filter featuring single-to-dual operation is presented. A multi-band bandstop filter with center frequency tunability achieved by varactor diodes is reported in [17, 18]. A multi-band miniaturized absorptive band-stop filter design based on the bridged-T coil was proposed in [19]. This method is adopted in [20] for the design of a miniaturized dual-band absorptive band-stop filter, and the structure exhibits improved passband performance. Recently, a planar dual-band absorptive band-stop filter based on coupled lines is reported in [21], which exhibits a high-selectivity dual-band stopband function and excellent absorptive characteristics. Therefore, investigations on dual-band and multi-band absorptive band-stop filters are not only important but also highly challenging.

For the purpose of meeting the requirements for absorptive behavior and dual-band operation, a novel absorptive bandstop filter configuration based on transmission lines is proposed in this paper. This structure features four transmission zeros, freely designable parameters, high-selectivity dual-band bandstop function. The main components of the absorptive bandstop filter include four transmission line branches and a main transmission path cascaded by four segments of transmission lines. A stepped-impedance branch is introduced into each of the four branches to increase the transmission zeros at the stopband center frequencies without affecting the dual-band absorption performance. Detailed circuit analysis and design procedures are provided in this paper. Lastly, a standard microstrip prototype is developed, simulated, and tested to validate the feasibility of the proposed concept.

2. ABSORPTIVE BANDSTOP FILTER DESIGN

As shown in Fig. 1(a), the topological structure of the planar absorptive band-stop filter is demonstrated. It is divided into three parts. The first part consists of four cascaded microstrip transmission lines forming the main transmission path. The second part consists of two parallel open-circuited stub sections, each section formed by cascading two microstrip transmission lines. The third part comprises two parallel microstrip transmission line stubs that are connected to resistors, respectively, and positioned close to the input port.

The filter's dual-band stopband performance is demonstrated in Fig. 2(a). As shown in Fig. 1, two resistor branches are introduced into the topology to achieve return loss absorption while maintaining dual-band stopband performance. After the introduction of the resistor branches, as illustrated in Fig. 2(b), the return loss within both stopbands is significantly lower than -15 dB.

When the values of R_1 and R_2 are both infinite, the two parallel resistor branches adjacent to Port 1 are open-circuited. At this point, the circuit is equivalent to that shown in Fig. 1(b). All energy is reflected back to Port 1 and not dissipated by the

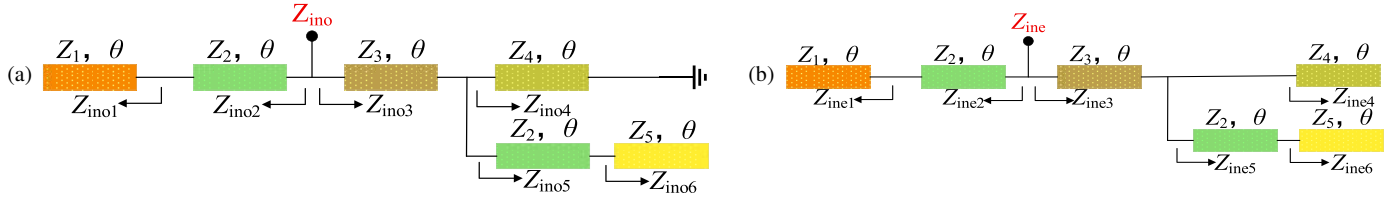

FIGURE 3. (a) Odd-mode equivalent circuit. (b) Even-mode equivalent circuit.

resistors. However, by properly adjusting the values of R_1 and R_2 to match these two parallel resistor branches with the input impedance of Port 1, energy is dissipated through the two resistor branches and not reflected back to Port 1. As shown in Fig. 1(b), the parallel stepped-impedance structure is introduced to generate transmission zeros.

3. THEORETICAL ANALYSIS

As depicted in Fig. 1(a), the two halves of the circuit are mirror images of each other with respect to the central vertical line. To facilitate theoretical analysis, odd-mode and even-mode equivalent circuits are respectively derived for this circuit topology. Specifically, the odd-mode equivalent circuit is illustrated in Fig. 3(a), while the even-mode counterpart is presented in Fig. 3(b). In Fig. 3(a), the characteristic impedances of all transmission lines are represented as Z_i $(i = 1, 2, 3, 4, 5)$, θ as the electrical length of all transmission lines, and Z_{ino1}, Z_{ino2}, Z_{ino3}, Z_{ino4}, Z_{ino5} as the input impedance of the odd-mode equivalent circuit.

Based on the transmission line theory, the input impedance Equation (1) of the even-mode equivalent circuit can be derived.

$$\begin{cases} Z_{ino1} = -jZ_1\cot\theta \\ Z_{ino2} = \frac{j\left(Z_2\tan^2\theta - Z_1\right)Z_2}{(Z_1+Z_2)\tan\theta} \\ Z_{ino3} = \frac{jZ_3^2(Z_{ino4}+Z_{ino5})\tan\theta + Z_3Z_{ino4}Z_{ino5}}{jZ_{ino4}Z_{ino5}\tan\theta + (Z_{ino4}+Z_{ino5})Z_3} \\ Z_{ino4} = jZ_4\tan\theta \\ Z_{ino5} = \frac{j\left(Z_2\tan^2\theta - Z_5\right)Z_2}{(Z_2+Z_5)\tan\theta} \\ Z_{ino6} = -jZ_5\cot\theta \end{cases} \tag{1}$$

Similarly, Equation (2) for the even-mode equivalent circuit can be obtained

$$\begin{cases} Z_{ine1} = -jZ_1\cot\theta \\ Z_{ine2} = \frac{j\left(Z_2\tan^2\theta - Z_1\right)Z_2}{(Z_1+Z_2)\tan\theta} \\ Z_{ine3} = \frac{jZ_3^2(Z_{ine4}+Z_{ine5})\tan\theta + Z_3Z_{ine4}Z_{ine5}}{jZ_{ine4}Z_{ine5}\tan\theta + (Z_{ine4}+Z_{ine5})Z_3} \\ Z_{ine4} = -jZ_4\cot\theta \\ Z_{ine5} = \frac{j\left(Z_2\tan^2\theta - Z_5\right)Z_2}{(Z_2+Z_5)\tan\theta} \\ Z_{ine6} = -jZ_5\cot\theta \end{cases} \tag{2}$$

The final Equation (3) for the odd-mode and even-mode input impedances can be derived.

$$\begin{cases} Z_{ino} = \frac{Z_{ino2}Z_{ino3}}{Z_{ino2}+Z_{ino3}} = \\ \quad \frac{\left(Z_1Z_2\tan\theta - Z_2^2\tan^3\theta\right)\left(A\tan^2\theta - B\right)}{j\left(Z_2^2\tan^2\theta - Z_1Z_2\right)C + j(A\tan^2\theta - B)(Z_1\tan^2\theta + Z_2\tan^2\theta)} \\ Z_{ine} = \frac{Z_{ine2}Z_{ine3}}{Z_{ine2}+Z_{ine3}} = \\ \quad \frac{j\left(Z_2^2\tan^2\theta - Z_1Z_2\right)\left(Z_3E - Z_3^2D\tan^2\theta\right)}{\tan\theta\left[(Z_1+Z_2)\left(Z_3E - Z_3^2D\tan^2\theta\right) - \left(Z_2^2\tan^2\theta - Z_1Z_2\right)(Z_3D+E)\right]} \end{cases} \tag{3}$$

The expressions for A, B, C, D, and E in Equation (3) are given in Equation (4).

$$\begin{cases} A = Z_3^2\left(Z_2Z_4 + Z_4Z_5 + Z_2^2\right) + Z_2^2Z_3Z_4 \\ B = Z_2Z_3Z_5\left(Z_3 + Z_4\right) \\ C = \left[Z_3\left(Z_2Z_4 + Z_4Z_5 + Z_2^2\right) + Z_2Z_4Z_5 \right. \\ \quad \left. - Z_2^2Z_4\tan^2\theta\right]\tan^2\theta - Z_2Z_3Z_5 \\ D = Z_2^2\tan^2\theta - Z_2Z_4 - Z_2Z_5 - Z_4Z_5 \\ E = Z_2Z_4\left(Z_2\tan^2\theta - Z_5\right) \end{cases} \tag{4}$$

The S_{11} and S_{21} are calculated in Equation (5) and Equation (6)

$$S_{11} = \frac{Z_0^2 - Z_{ine}Z_{ino}}{\left(Z_{ino}+Z_0\right)\left(Z_{ine}+Z_0\right)} \tag{5}$$

$$S_{21} = \frac{Z_0\left(Z_{ine} - Z_{ino}\right)}{\left(Z_{ino}+Z_0\right)\left(Z_{ine}+Z_0\right)} \tag{6}$$

The transmission zeros can be achieved when S_{21} equals zero.

By analogy, there are two cases: one is that Z_{ino} equals Z_{ine} and neither is infinite, and the other is that both Z_{ino} and Z_{ine} are infinite.

Case 1.

$$Z_{ino} = Z_{ine} \neq \infty \tag{7}$$

Case 2.

$$\begin{cases} Z_{ino} = \infty \\ Z_{ine} = \infty \end{cases} \tag{8}$$

All transmission zeros can be obtained through case 1 and case 2.

$$\begin{cases} \tan\theta\left(f_{tz1}\right) \approx 0.618 \\ \tan\theta\left(f_{tz2}\right) \approx 0.823 \end{cases} \tag{9}$$

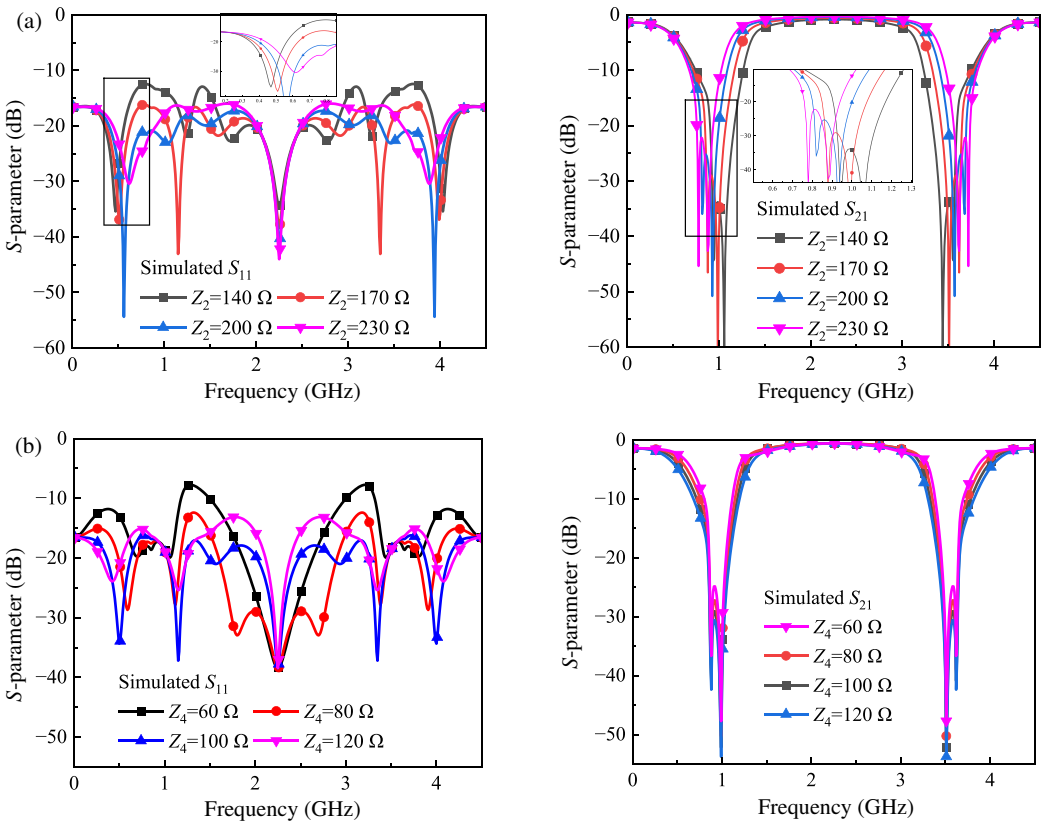

FIGURE 4. Simulation results of S_{11} and S_{21} with different values of Z_2 and Z_4. (a) With different values of Z_2. (b) With different values of Z_4.

As shown in Equation (10), a total of four solutions for θ within the range of 0 to π can be obtained from Equation (9).

$$\begin{cases} \theta\left(f_{tz1}\right) = \arctan 0.618 \\ \theta\left(f_{tz2}\right) = \arctan 0.823 \\ \theta\left(f_{tz3}\right) = \pi - \theta\left(f_{tz2}\right) \\ \theta\left(f_{tz4}\right) = \pi - \theta\left(f_{tz1}\right) \end{cases} \tag{10}$$

The positions of the four transmission zeros can be determined through Equation (11). f_0 denotes the center frequency.

$$f_{tzn} = \frac{2f_0}{\pi}\theta\left(f_{tzn}\right), \quad (n = 1, 2, 3, 4) \tag{11}$$

Simulations are conducted through ADS software when different values are selected for Z_2 and Z_4. Fig. 4 illustrates that Z_2 and Z_4 affect the return loss in passbands. In Fig. 4(a), the value of Z_2 exerts a significant influence on the return loss outside the two stopbands, while it has a relatively minor impact on the passband bandwidth. However, in Fig. 4(b), the value of Z_4 primarily affects the return loss within the two stopbands as well as the passband bandwidth notably. Specifically, as the value of Z_2 increases, the passband bandwidth expands. Therefore, to achieve the optimal overall performance, the filter configuration adopted in this paper is the value of Z_4 which is 100 Ω, and the value of Z_2 is 170 Ω. In order to achieve the best results, the circuit parameters are as follows: $Z_1 = 116\,\Omega$, $Z_2 = 170\,\Omega$, $Z_3 = 56\,\Omega$, $Z_4 = 100\,\Omega$, $Z_5 = 84\,\Omega$, $\theta = 40°$, $R_1 = 300\,\Omega$, $R_2 = 275\,\Omega$.

EM simulation results of S_{11} and S_{21} with different values of R are shown in Fig. 5. Fig. 5(a) characterizes the influence of the variation of R_1 on the S-parameter curves when R_2 is a fixed value, while Fig. 5(b) characterizes the influence of the variation of R_2 on the S-parameter curves when R_1 is a fixed value. As can be seen from Fig. 5(a), with the increase of R_1, the return loss S_{11} in the first stopband shows an overall decreasing trend, and the maximum return loss S_{11} at the center frequency within this stopband can reach −18 dB. However, as R_1 increases, the return loss S_{11} at the center frequency of the second stopband presents an overall increasing trend, and the maximum return loss S_{11} at the center frequency within this stopband can reach −12 dB.

It can be observed from Fig. 5(b) that with the increase of R_2, the return loss S_{11} in the first stopband exhibits an overall increasing trend, and the maximum return loss S_{11} within this stopband can reach −12 dB; the insertion loss S_{21} in the second stopband decreases gradually, and the transmission zeros near the center frequency of this stopband shifts or disappears.

From the above observations, it can be concluded that the return loss S_{11} in the two stopbands are affected simultaneously by R_1 and R_2, and the transmission zeros near the center frequency of this stopband shift or disappear depending on the value of R_2. This also verifies the absorption function of R_1 and R_2 on the return loss S_{11}.

The absorptive band-stop filter incorporates two stopbands with center frequencies of 0.92 GHz and 3.58 GHz, respectively (center frequency $f_0 = 2.25$ GHz, $\theta = 40°$).

TABLE 1. Performance comparison of the ABSF.

Filter structures	Number of stopbands	FBWs (% @dB)	Center frequency (GHz)	Number of transmission zeros	Return loss at stopbands (dB)
Ref. [9]	1	-	2.00	1	> 10.00
Ref. [19]	2	58.30/30.50 @−3 21.80/11.90 @−10	4.80/9.60	2	21.90/12.80
Ref. [20]	2	60.30/37.70 @−3 22.70/14.00 @−10	4.80/9.60	2	15.90/10.10
Ref. [21]	2	54.54/67.42 @−3 30.42/13.87 @−10	0.63/1.37	2	13.30/14.70
Ref. [22]	2	34.9/25.9 @−3 14.93/10.69 @−10	0.68/1.28	2	> 10.00
This work	**2**	**115.79/34.87 @−3 50.27/13.18 @−10**	**0.92/3.58**	**4**	**22.36/11.11**

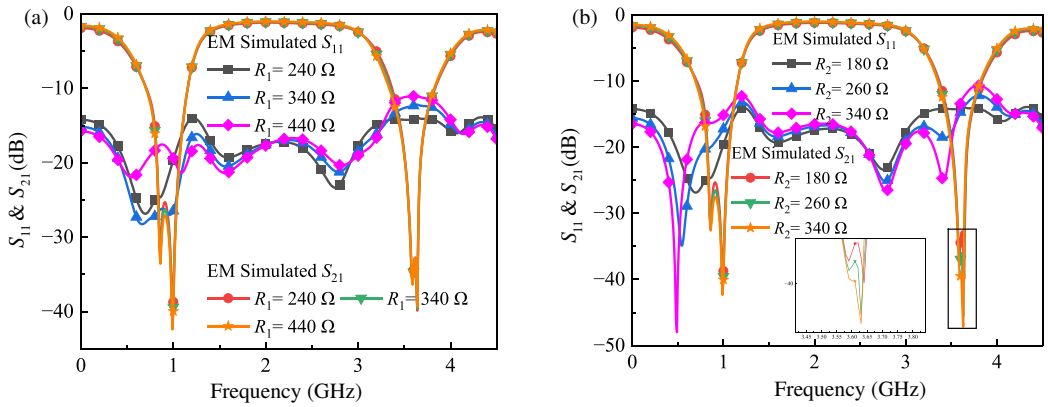

FIGURE 5. EM simulation results of S_{11} and S_{21}. (a) With different values of R_1. (b) With different values of R_2.

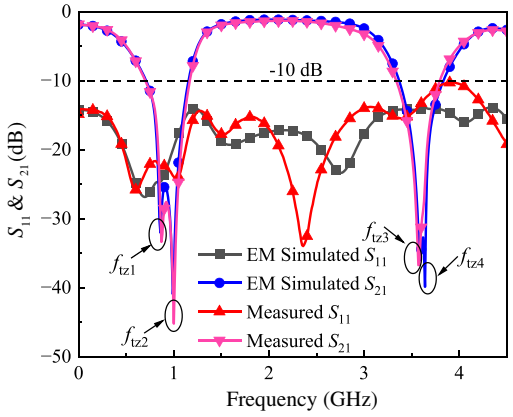

FIGURE 6. EM simulated and measured results.

The filter prototype is fabricated on an RO4350B substrate, which has a dielectric constant of 3.66, a loss tangent of 0.0037, and a copper foil thickness of 1.524 mm. The circuit dimensions and a physical prototype photograph are presented in Fig. 8. The dimensions of the proposed filter are 10.2 cm × 2.6 cm ($0.77\lambda_0 \times 0.20\lambda_0$), where λ_0 denotes the free-space wavelength at the center frequency. The simulated and measured results of the filter are illustrated in Fig. 6, from which the bandwidths of the two stopbands can be observed.

For the stopband definition of $S_{21} < -10$ dB, the first stopband spans from 0.7 GHz to 1.17 GHz with a relative fractional bandwidth of 50.27%, while the second stopband ranges from 3.33 GHz to 3.80 GHz with a relative fractional bandwidth of 13.18%. For the definition of $S_{21} < -3$ dB, the first stopband covers the frequency range of 0.36 GHz to 1.35 GHz (relative fractional bandwidth: 115.79%), and the second stopband extends from 2.96 GHz to 4.21 GHz (relative fractional bandwidth: 34.87%). Within the first stopband, the maximum return loss S_{11} is −14.45 dB at 1.26 GHz, and the maximum insertion loss S_{21} reaches −27.58 dB at 0.91 GHz. In the second stopband, the maximum return loss S_{11} is −10.27 dB at 3.94 GHz, while the maximum insertion loss S_{21} attains −36.73 dB at 3.57 GHz.

As shown in Table 1, comparisons are conducted. The proposed filter is compared with other filters in Table 1. Its novelty is verified: multiple transmission zeros and dual-bandstop absorptive performance are simultaneously achieved. Additionally, the −3 dB relative bandwidth of the first stopband reaches 115.79%.

As shown in Fig. 5 and Fig. 7, EM simulation results of S_{11} and S_{21} with different values of R are presented. With variations in the resistance value, the transmission zeros are likely to

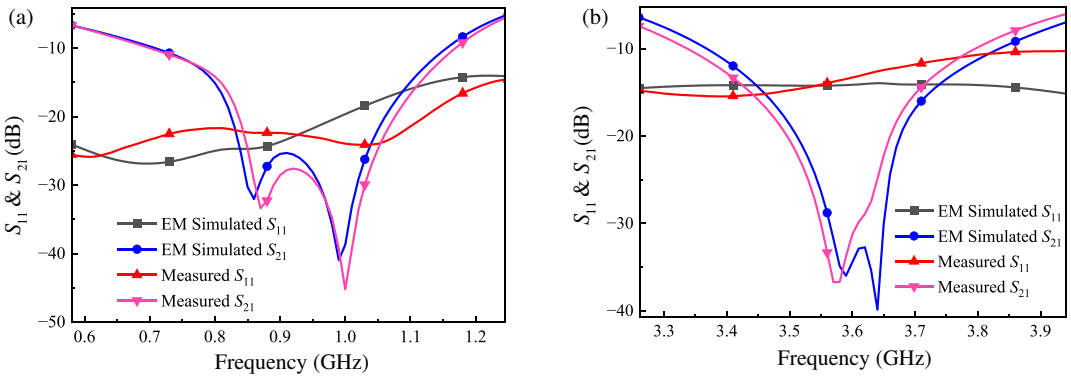

FIGURE 7. EM simulated and measured results. (a) The first band. (b) The second band.

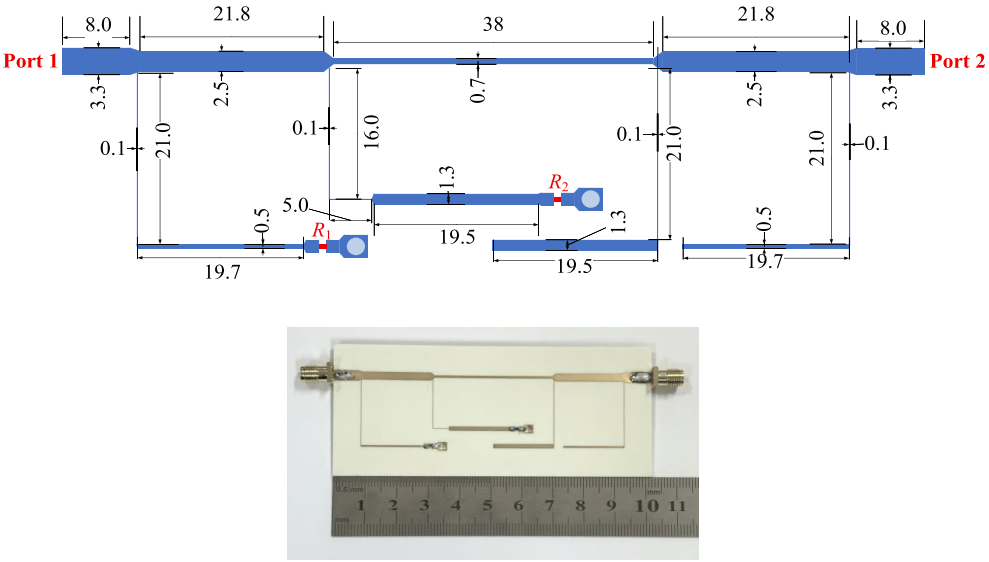

FIGURE 8. The layout dimensions and physical photograph of the proposed filter (Unit: mm).

shift or vanish within the operating frequency. In addition, the precision of processing, the accuracy of chip resistors, and the errors during actual measurement may cause individual transmission zeros to shift or disappear.

4. CONCLUSION

In this paper, a novel planar dual-band absorptive band-stop filter (ABSF) based on transmission lines is proposed. The filter structure is composed of multiple transmission lines and two chip resistors, which endows it with distinct advantages, including four transmission zeros, high-selectivity dual-bandstop performance. To accurately characterize its frequency response, detailed formula derivations are conducted, through which the specific positions of the four transmission zeros within the operating frequency are precisely determined. The physical dimensions of the filter is 102 mm $\times$ 26 mm ($0.77\lambda_0 \times 0.20\lambda_0$).

ACKNOWLEDGEMENT

This work was supported by the National Natural Science Foundation of China (62201065).

REFERENCES

[1] Gu, Y., S. Xue, W. Sun, T. Xie, X. Wang, and C.-P. Chen, "A reconfigurable single-/dual-bandstop filter with controllable equal-ripple performance," *Applied Sciences*, Vol. 14, No. 13, 5837, 2024.

[2] Cai, T., C. Chen, and F. Lin, "Single and multiband bandstop filters with hybrid transmission-line/SAW-resonator transversal filtering sections," in *2023 International Conference on Microwave and Millimeter Wave Technology (ICMMT)*, 1–3, Qingdao, China, 2023.

[3] Yang, D., H. Tian, and Y. Dong, "Miniaturized reciprocal DMS-DGS unit and its application to single-/dual-band bandstop filters," *IEEE Transactions on Circuits and Systems II: Express Briefs*, Vol. 70, No. 12, 4299–4303, 2023.

[4] Kalyanarao, B. and R. R. Reddy, "Lumped-element based tunable bandstop filter for airborne UHF communication system," in *2023 IEEE Wireless Antenna and Microwave Symposium (WAMS)*, 1–4, Ahmedabad, India, 2023.

[5] Elabd, R. H., "Compact dual-port MIMO filtenna-based DMS with high isolation for C-band and X-band applications," *EURASIP Journal on Wireless Communications and Networking*, Vol. 2023, No. 1, 110, 2023.

[6] Elabd, R. H. and A. H. Hussein, "Efficient design of a wideband tunable microstrip filtenna for spectrum sensing in cognitive radio systems," *EURASIP Journal on Wireless Communications and Networking*, Vol. 2023, No. 1, 109, 2023.

[7] Lu, Q., X. Wu, and C. Wang, "Compact broadband absorptive bandstop filter based on microstrip," *Journal of Physics: Conference Series*, Vol. 1651, No. 1, 012104, 2020.

[8] Lee, J. and J. Lee, "Distributed-element reflectionless bandstop filter with a broadband impedance matching," *IEEE Microwave and Wireless Components Letters*, Vol. 30, No. 6, 561–564, 2020.

[9] Lee, J. and J. Lee, "Transmission-line absorptive bandstop filters with wide passband: Synthesis and design," *IEEE Transactions on Microwave Theory and Techniques*, Vol. 69, No. 12, 5371–5380, 2021.

[10] Kong, M., Y. Wu, Z. Zhuang, W. Wang, and C. Wang, "Ultra-miniaturized wideband input-absorptive bandstop filter based on TFIPD technology," *IEEE Transactions on Circuits and Systems II: Express Briefs*, Vol. 68, No. 7, 2414–2418, 2021.

[11] Zhao, K. and D. Psychogiou, "X-band MMIC-based tunable quasi-absorptive bandstop filter," *IEEE Microwave and Wireless Technology Letters*, Vol. 33, No. 4, 391–394, 2023.

[12] Kong, M., Y. Wu, Z. Zhuang, Y. Liu, and A. A. Kishk, "Compact wideband reflective/absorptive bandstop filter with multi-transmission zeros," *IEEE Transactions on Microwave Theory and Techniques*, Vol. 67, No. 2, 482–493, 2019.

[13] Hickle, M. D. and D. Peroulis, "Theory and design of frequency-tunable absorptive bandstop filters," *IEEE Transactions on Circuits and Systems I: Regular Papers*, Vol. 65, No. 6, 1862–1874, 2017.

[14] Lee, T.-H., J.-J. Laurin, and K. Wu, "Reconfigurable filter for bandpass-to-absorptive bandstop responses," *IEEE Access*, Vol. 8, 6484–6495, 2020.

[15] Zahari, M. K., B. H. Ahmad, W. P. Wen, and N. A. Shairi, "Switchable absorptive bandstop to bandpass filter using dual-mode ring resonator," in *2016 IEEE Asia-Pacific Conference on Applied Electromagnetics (APACE)*, 248–251, Langkawi, Malaysia, 2016.

[16] Şahin, E. G., "A reconfigurable and tunable single to dual wideband bandstop filter by using nested dual-mode square loop resonators," *AEU — International Journal of Electronics and Communications*, Vol. 168, 154710, 2023.

[17] Gorur, A. K. and D. Psychogiou, "Single-/dual-band bandpass-to-bandstop filters with center frequency tunability," *IEEE Access*, Vol. 12, 90 697–90 706, 2024.

[18] Bayati, M. S., S. M. H. Mousavi, and S. V. A.-D. Makki, "Combination of absorptive notch filter and tunable dual-band conventional notch filter," *Microwave and Optical Technology Letters*, Vol. 64, No. 1, 30–35, 2022.

[19] Chang, E.-W. and Y.-S. Lin, "Miniature multi-band absorptive bandstop filter designs using bridged-T coils," *IEEE Access*, Vol. 6, 73 637–73 646, 2018.

[20] Lin, Y.-S., Y.-C. Huang, and Q.-Y. Jiang, "Miniature dual-band absorptive bandstop filters with improved passband performance," *IEEE Transactions on Circuits and Systems I: Regular Papers*, Vol. 69, No. 6, 2339–2350, 2022.

[21] Zuo, X., L. Qin, M. He, H. Mei, and Y. Li, "Planar dual-band coupled-line absorptive bandstop filter with an input lossy step-impedance stub," *AEU — International Journal of Electronics and Communications*, Vol. 176, 155133, 2024.

[22] Mei, H. and X. Zuo, "A dual-band input-apsorptive bandstop filter using coupled lines," in *2023 International Applied Computational Electromagnetics Society Symposium (ACES-China)*, 1–3, Hangzhou, China, Aug. 2023.